energies

MDPI

Thermal Transport in Nonlinear Unsteady Colloidal Model by Considering the Carbon Nanomaterials Length and Radius

Syed Tauseef Mohyud-Din [1], Adnan [2], T. Abdeljawad [3,4,5], Umar Khan [6], Naveed Ahmed [7] and Ilyas Khan [8,*]

[1] University of Multan, Multan 60000, Pakistan; syedtauseefs@hotmail.com
[2] Department of Mathematics, Mohi-ud-Din Islamic University, Nerian Sharif AJ&K, Trarkhel 12080, Pakistan; adnan_abbasi89@yahoo.com
[3] Department of Mathematics and General Sciences, Prince Sultan University, Riyadh 11586, Saudi Arabia; tabdeljawad@psu.edu.sa
[4] Department of Medical Research, China Medical University, Taichung 40402, Taiwan
[5] Department of Computer Science and Information Engineering, Asia University, Taichung 40704, Taiwan
[6] Department of Mathematics and Statistics, Hazara University, Mansehra 21120, Pakistan; umar_jadoon4@yahoo.com
[7] Department of Mathematics, Faculty of Sciences, HITEC University, Taxila Cantt 47070, Pakistan; nidojan@gmail.com
[8] Faculty of Mathematics and Statistics, Ton Duc Thang University, Ho Chi Minh City 72915, Vietnam
* Correspondence: ilyaskhan@tdtu.edu.vn

check for updates

Abstract: Thermal transport analysis in colloidal suspension is significant from industrial, engineering, and technological points of view. It has numerous applications comprised in medical sciences, chemical and mechanical engineering, electronics, home appliances, biotechnology, computer chips, detection of cancer cells, microbiology, and chemistry. The carbon nanomaterials have significant thermophysical characteristics that are important for thermal transport. Therefore, the thermal transport in H_2O composed by single and multiwalled carbon nanotubes is examined. The length and radius of the nanomaterials is in range of 3 μm ≤ L* ≤ 70 μm and 10 nm ≤ d ≤ 40 nm, respectively. The problem is modelled over a curved stretching geometry by inducing the velocity slip and thermal jump conditions. The coupling of Runge-Kutta (RK) and shooting technique is adopted for the solution. From the analysis it is perceived that the heat transfer at the surface drops for stretching. The heat transfer rate prevailed for Single walled carbon nanotubes SWCNTs-H_2O colloidal suspension. The suction and stretching of the surface resist the shear stresses and more shear stress trends are investigated for larger curvature.

Keywords: thermal transport; curved surface; carbon nanotubes; thermophysical characteristics; curvature; RK scheme

1. Introduction

The heat transfer analysis in the nanofluids attained much interest of researchers, engineers, and industrialists. Nanofluids are newly engineered fluids with potential heat transfer characteristics. A fluid composed by the tiny particles of the metals and their oxides and host liquids is called a nanofluid. Thermal conductivity is significant in the nanofluids for heat transfer due to high thermal conductance of the tiny particles of various metals and oxides. Therefore, Maxwell [1] thought that thermal transport characteristics could be enhanced and proposed a theoretical thermal conductance correlation.

At the end of 19th century, Choi [2] extended the thought of Maxwell and introduced the word "nanofluid". The metals and their oxides, Carbon nanotubes (CNTs) and ferro magnetics tiny materials have high thermal conductance. Therefore, the heat transfer in the regular liquids could be improved by dispersing these tiny particles. Due to high thermal transport characteristics, nanofluids gained popularity in different areas of engineering and industries. The applications of nanofluids in nanotechnology, biomedical sciences, chemical engineering, include detecting cancer cells in the human body, use in home appliances, electronics, civil engineering, botany, and many other fields of research.

A thermal conductivity correlation based on the shapes of tiny particles (cylinders, bricks, and blades) was proposed by Hamilton [3]. Bruggemann [4] familiarized the correlation for high volume fraction of the spherical tiny particles. Wasp [5] modified the correlation of Hamilton [3] for shape factor n = 3. Koo and Kleinstreuer [6,7] developed a correlation for CuO diluted in the two separate host liquids known as ethylene glycol and oil. Influences of the temperature on the behavior of thermal conductivity of Al_2O_3-H_2O and CuO-H_2O colloidal mixture was revealed in [8]. A reliable thermal conductivity correlation for metallic and oxides based nanoliquids was developed by Patel et al. [9]. They plugged the tiny particles diameter and temperature influences into the thermal conductance of the nanoliquid. A compatible thermal conductivity correlation for Ag-H_2O nanoliquid was constructed by Godson et al. [10]. Corcione [11] contributed the improvement in heat transfer for Al_2O_3-H_2O nanofluid by incorporating the influences of freezing temperature in the thermal conductance correlation.

The researchers, engineers, scientists, and industries were inspired by the heat transport characteristics in the nanofluids. Therefore, they started to analyze the behavior of nanofluids velocity, and temperature under various physical situations. Sheikholeslami et al. [12] perceived the nanofluid characteristics in a porous cavity. Further, they ingrained the influences of thermal radiations in a magnetized cavity for fascinating results regarding velocity and temperature. They found escalations in the nanofluid temperature in the occurrence of imposed radiative heat flux. The implementation of KKL thermal conductivity correlation in magnetized nanofluid was reported in [13]. 3D flow of γ Al_2O_3-H_2O and γ Al_2O_3-$C_2H_6O_2$ colloidal suspensions squeezed between parallel magnetized plates was examined in [14]. The lower plate is stationary at y = 0 and upper plate is at y = h(t). The nanofluids squeezed between the plates due to the downwards movement of the upper plate. They implemented a numerical technique for the mathematical treatment of the models and explored the results for thermal transport in the nanofluids under various physical situations. They found significant behavior of the particular nanofluids for squeezing effects. The impacts of effective Prandtl model and thermal radiations on the flow of nanofluids and viscous regular liquid was detected in [15,16] between rotating plates and oblique walls, respectively.

Like nanoparticles, another solid material known as carbon nanotubes was introduced in [17] that have high thermal conductivity and are widely used in material science, nanotechnology, optics, and in electronics. These are subcategorized as single (SWCNTs) and multi-walled (MWCNTs) carbon nanotubes. Due to unique mechanical and thermal properties, the colloidal study of carbon nanotubes attained huge interest of researchers and scientists. To intensify thermal conductivity of the carbon nanotubes, several models were proposed described in [18,19]. Therefore, researchers studied the temperature behavior in the nanoliquids composed by carbon nanomaterials.

Nadeem et al. [20] described theoretical analysis for the heat transport in the nanoliquids suspended by SWCNTs and MWCNTs nanotubes. Additionally, they encountered the influences of wavy wall conditions in the flow regimes. Thermal radiations and velocity slip condition effects on the nanoliquid flow between Riga geometry and oblique walls were presented in [21,22], respectively. They used carbon nanomaterials in the host liquid for thermal improvement and found fascinating results. The analysis of carbon nanomaterials based nanofluids over curved stretchable geometry was decorated in [23]. Nonlinear thermal radiative flux and cross diffusion gradients on the nanoliquid flow over a curved surface was detected in [24]. Similarly, Saleh et al. [25] highlighted the flow regimes

for micropolar fluid flow over an arched stretching/shrinking surface with permeable effects. 3D flow for stretching plate, flow over stretching cylinder, and boundary layer study over solid surface were described in [26–28], respectively.

It is clear that the analysis of thermal transport by incorporating the length and radius effects of carbon nanomaterials in the host liquid has not been attempted so far. Therefore, this analysis was carried out to fill this significant gap in the research field. The effects of velocity are incorporated in the flow conditions and the model treated numerically. Further, the results for the nanofluid velocity behavior, local thermal transport, and shear stresses for various flow parameters are decorated and discussed comprehensively in the presented analysis.

2. Materials and Methods

2.1. Model Formulation

2.1.1. Statement and Geometry of the Model

The colloidal composition of CNTs-H_2O nanofluid is considered over an arched surface with stretching property in curvilinear frame. It is assumed that the nanofluid obeys the characteristics of incompressibility. The radius of the surface is denoted by R and it is placed in a (r, s) coordinate system. The surface has stretching or shrinking properties with velocity U_w which varies along the surface. Moreover, the velocity V_w depends on s and t represents the injecting fluid for $V_w > 0$ and suction of the fluid for $V_w < 0$. Figure 1 elaborates the flow situation for the consideration nanofluid.
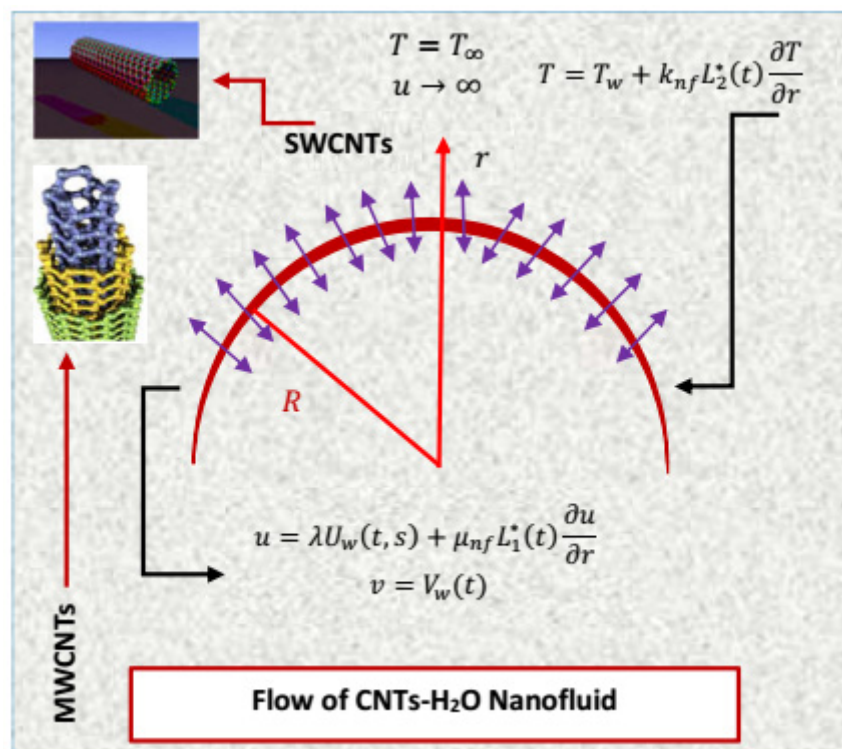

Figure 1. Flow of CNTs-H_2O colloidal suspension over curved stretching/shrinking surface.

2.1.2. Governing Model and Similarity Transformations

The following unsteady nondimensional flow model represents the nanofluid flow of CNTs-H2O over a curved surface [29].

$$\frac{\partial}{\partial r}\left(\breve{v}\left(r + \breve{R}\right)\right) + \breve{R}\frac{\partial \breve{u}}{\partial S} = 0, \tag{1}$$

$$\breve{u}^2\left(r+\breve{R}\right)^{-1} = \frac{\partial \breve{p}}{\partial r}\left(\breve{\rho}_{cnt}\right)^{-1}, \tag{2}$$

$$\frac{\breve{\mu}_{cnt}}{\breve{\rho}_{cnt}}\left(\frac{\partial^2 \breve{u}}{\partial r^2} + \left(r+\breve{R}\right)^{-1}\frac{\partial \breve{u}}{\partial r} - \breve{u}\left(r+\breve{R}\right)^{-2}\right) + \frac{1}{\breve{\rho}_{cnt}}\left(\breve{R}\left(r+\breve{R}\right)^{-1}\frac{\partial \breve{p}}{\partial S}\right)$$
$$= \frac{\partial \breve{u}}{\partial t} + \breve{v}\frac{\partial \breve{u}}{\partial r} + \breve{R}\breve{u}\left(r+\breve{R}\right)^{-1}\frac{\partial \breve{u}}{\partial S} + \breve{u}\breve{v}\left(r+\breve{R}\right)^{-1}, \tag{3}$$

$$\frac{\partial \breve{T}}{\partial t} + \breve{v}\frac{\partial \breve{T}}{\partial r} + \breve{u}\breve{R}\left(r+\breve{R}\right)^{-1}\frac{\partial \breve{T}}{\partial S} = \frac{\breve{k}_{cnt}}{\left(\overline{\rho c_p}\right)_{cnt}}\left(\frac{\partial^2 \breve{T}}{\partial r^2} + \left(r+\breve{R}\right)^{-1}\frac{\partial \breve{T}}{\partial r}\right) \tag{4}$$

The conditions at the surface and at the free surface are:

$$\left.\begin{array}{l} \breve{u} = 0 \\ \breve{v} = 0 \quad \text{for any r and s and } t < 0 \\ \breve{T} = T_\infty \end{array}\right\}, \tag{5}$$

$$\left.\begin{array}{l} \breve{v} = V_w(t) \\ \breve{u} = \lambda U_w + \breve{\mu}_{nf}L_1^*\frac{\partial u}{\partial r} \text{ for } t \geq 0 \\ \breve{T} = T_w + \breve{k}_{nf}L_2^*\frac{\partial \breve{T}}{\partial r} \text{ at } r = 0 \\ \breve{u} \to 0, \quad \frac{\partial \breve{u}}{\partial r} \to 0, \quad \breve{T} \to T_\infty \text{ as } r \to \infty \end{array}\right\}, \tag{6}$$

In Equation (6), the velocities $U_w = as\left(1-\alpha t\right)^{-1}$, $V_w = -a\nu_f\left(1-\alpha t\right)^{-1}S$ are s and t dependent, surface stretching and shrinking is represented by $\lambda < 0$ and $\lambda > 0$, respectively. The accelerated and decelerated flow situations depend on the value of α. The positive α shows the accelerating and negative α corresponds to decelerating flow situation. Further, suction or injection of the nanofluid denoted by S and L_1^* and L_2^* are the temperature jump and velocity slip parameters, respectively.

For nondimensionalization of the model, the following are defined similarities [29]:

$$\left.\begin{array}{l} \eta = \sqrt{\frac{a\left(1-\alpha t\right)^{-1}}{\nu_{bf}}}r \\ \breve{v} = -\breve{R}\left(r+\breve{R}\right)^{-1}\sqrt{a\nu_{bf}\left(1-\alpha t\right)^{-1}}L(\eta) \\ \breve{u} = as\left(1-\alpha t\right)^{-1}L\prime(\eta) \\ \breve{p} = \breve{\rho}_f(as)^2\left(1-\alpha t\right)^{-2}\breve{p}(\eta) \\ \breve{N}(\eta) = \frac{T-T_\infty}{T_w-T_\infty} \end{array}\right\} \tag{7}$$

2.1.3. Effective Nanofluid Models

To improve the thermophysical characteristics, the following models are utilized [20]:

$$\breve{\rho}_{nf} = \left[(1-\phi) + \frac{\phi\breve{\rho}_{cnt}}{\breve{\rho}_f}\right]\breve{\rho}_f, \tag{8}$$

$$\left(\overline{\rho C_p}\right)_{nf} = \left[(1-\phi) + \frac{\phi\left(\overline{\rho C_p}\right)_{cnt}}{\left(\overline{\rho C_p}\right)_f}\right]\left(\overline{\rho C_p}\right)_f, \tag{9}$$

$$\breve{\mu}_{nf} = \breve{\mu}_f(1-\phi)^{-2.5}. \tag{10}$$

$$\breve{k}_{nf} = \frac{\breve{k}_f\left(1 - \frac{\breve{k}_f}{\breve{k}_s}\frac{L}{\breve{R}}\,\phi^{0.2} + \left(1 - \frac{\breve{k}_f}{\breve{k}_s}\right)\phi\frac{L}{\breve{R}}\,\phi^{0.2} + 2\,\phi\frac{\breve{k}_s}{\breve{k}_s - \breve{k}_f}\ln\left(\frac{\breve{k}_s + \breve{k}_f}{2\,\breve{k}_f}\right)\right)}{1 - \phi + 2\,\phi\left(\frac{\breve{k}_s}{\breve{k}_s - \breve{k}_f}\right)\ln\left(\frac{\breve{k}_s + \breve{k}_f}{2\,\breve{k}_f}\right)} \tag{11}$$

where, $\breve{\rho}_{nf}$ is the density, $\left(\overline{\rho \breve{C}_p}\right)_{nf}$ heat capacitance, $\breve{\mu}_{nf}$, dynamic viscosity, and $\breve{k}_{nf}$ is the effective thermal conductivity of the nanofluid. Further, $\breve{\rho}_f$, $\breve{\mu}_f$, $\breve{k}_f$ are the density, dynamic viscosity, and thermal conductivity of the fluid phase and $\breve{k}_s$ is thermal conductivity of the carbon nanotubes. The volume fraction is ϕ and the length and radius of the Carbon nanotubes (CNTs) are L and R, respectively. The thermal and physical characteristics of the fluid phase and carbon nanotubes are described in Table 1.

Table 1. Thermophysical characteristics of CNTs and H_2O.

Properties	$\breve{\rho}(kg/m^3)$	$\overline{\breve{c}_p}(J/Kg\ K)$	$\overline{\breve{k}}(W/mk)$	$\breve{\sigma}(S/m)$
H_2O	997.1	4179	0.613	0.005
SWCNTs	2600	425	6600	——
MWCNTs	1600	796	3000	——

2.1.4. Nondimensional Nanofluid Model

With the help of Equation (11), Equations (1)–(4) are transformed into the following model in the presence of length and radius of the carbon nanotubes incorporating in the energy equation:

$$L'''' + \frac{2}{K+\eta}L''' + (K+\eta)^{-3}L' + \frac{(1-\phi)+\frac{\phi\breve{\rho}_{cnt}}{\breve{\rho}_f}}{(1-\phi)^{-2.5}}$$
$$\left\{K(K+\eta)^{-1}\left(LL''' - L'L''+K(K+\eta)^{-2}\left(LL'' - L'^2\right)-K(K+\eta)^3LL' - \beta^*(K+\eta)^{-1}\left(L'+\frac{\eta}{2}L''\right)-\frac{\beta^*}{2}(3L''+\eta L''')\right\}= 0,$$

(12)

$$\left(\frac{1-\frac{\breve{k}_f}{\breve{k}_s}\frac{L}{R}\ \phi^{0.2}+\left(1-\frac{\breve{k}_f}{\breve{k}_s}\right)\phi\frac{L}{R}\ \phi^{0.2}+2\ \phi\frac{\breve{k}_s}{\breve{k}_s-\breve{k}_f}\ln\left(\frac{\breve{k}_s+\breve{k}_f}{2\ \breve{k}_f}\right)}{1-\phi+2\ \phi\left(\frac{\breve{k}_s}{\breve{k}_s-\breve{k}_f}\right)\ln\left(\frac{\breve{k}_s+\breve{k}_f}{2\ \breve{k}_f}\right)}\right)$$

(13)

$$\left(N'' + (K+\eta)^{-1}N'\right)-\left\{(1-\phi)+\frac{\phi\left(\overline{\rho\breve{C}_p}\right)_{cnt}}{\left(\overline{\rho\breve{C}_p}\right)_f}\right\}Pr\left(0.5N'\beta^* - K(K+\eta)^{-1}LN'\right) = 0.$$

The boundary conditions described in Equations (5) and (6) after the implementation of the similarity transformation reduced into the following version:

$$\left.\begin{array}{c}L(\eta) = S\\L'(\eta) = \lambda + \frac{1}{(1-\phi)^{2.5}}\ \lambda_1 L''(\eta)\\N(\eta) = 1+\left(\frac{1-\frac{\breve{k}_f}{\breve{k}_s}\frac{L}{R}\ \phi^{0.2}+\left(1-\frac{\breve{k}_f}{\breve{k}_s}\right)\phi\frac{L}{R}\ \phi^{0.2}+2\ \phi\frac{\breve{k}_s}{\breve{k}_s-\breve{k}_f}\ln\left(\frac{\breve{k}_s+\breve{k}_f}{2\ \breve{k}_f}\right)}{1-\phi+2\ \phi\left(\frac{\breve{k}_s}{\breve{k}_s-\breve{k}_f}\right)\ln\left(\frac{\breve{k}_s+\breve{k}_f}{2\ \breve{k}_f}\right)}\right)\lambda_2 N'(\eta)\\ \text{here, } \lambda_1 = L_1^*\ \sqrt{a\breve{\mu}_f\breve{\rho}_f(1-\alpha t)^{-1}}\\ \lambda_2 = L_2^*\sqrt{a\left(\breve{v}_f(1-\alpha t)\right)^{-1}\breve{k}_f}\\ \text{and } L_1^* = L_1\sqrt{1-t\alpha}\\ L_2^* = L_2\sqrt{1-t\alpha}\end{array}\right\}\text{at}\eta\ = 0,$$

(14)

$$\left.\begin{array}{c}L\prime(\eta) \to 0\\L''(\eta) \to 0\\N(\eta) \to 0\end{array}\right\}\text{ as }\eta \to \infty,$$

(15)

2.1.5. Significant Quantities from Engineering Aspects

The shear stresses and local Nusselt number can be defined by the formulas:

$$C_F = \tau_w \left(\breve{\rho}_f (as)^2 \right)^{-1} \text{ and } Nu = sq_w \left(\breve{k}_f (T - T_\infty) \right)^{-1} \tag{16}$$

Here, the wall shear stress and the wall heat flux are denoted by τ_w and q_w, respectively. These are as follows:

$$\left. \begin{array}{l} \tau = \breve{\mu}_{nf} \left(\dfrac{\partial \breve{u}}{\partial r} - \breve{u} \left(r + \breve{R} \right)^{-1} \right) \downarrow_{r=0} \\[3mm] q_w = - \left(\dfrac{1 - \frac{\breve{k}_f}{\breve{k}_s} \frac{L}{R} \, \phi^{0.2} + \left(1 - \frac{\breve{k}_f}{\breve{k}_s} \right) \phi \frac{L}{R} \, \phi^{0.2} + 2 \, \phi \frac{\breve{k}_s}{\breve{k}_s - \breve{k}_f} \ln \left(\frac{\breve{k}_s + \breve{k}_f}{2 \, \breve{k}_f} \right)}{1 - \phi + 2 \, \phi \left(\frac{\breve{k}_s}{\breve{k}_s - \breve{k}_f} \right) \ln \left(\frac{\breve{k}_s + \breve{k}_f}{2 \, \breve{k}_f} \right)} \right) \dfrac{\partial \breve{T}}{\partial r} \downarrow_{r=0} \end{array} \right\}. \tag{17}$$

Finally, the self-similar form for shear stress and local heat transfer are obtained in the following way:

$$\left. \begin{array}{l} C_F = \dfrac{\breve{\mu}_{nf}}{\breve{\mu}_f} \left(L''(0) \left(1 - \dfrac{\lambda_1 \breve{\mu}_{nf}}{\breve{\mu}_f K} \right) - \lambda K^{-1} \right) \\[3mm] Nu = - \left(\dfrac{1 - \frac{\breve{k}_f}{\breve{k}_s} \frac{L}{R} \, \phi^{0.2} + \left(1 - \frac{\breve{k}_f}{\breve{k}_s} \right) \phi \frac{L}{R} \, \phi^{0.2} + 2 \, \phi \frac{\breve{k}_s}{\breve{k}_s - \breve{k}_f} \ln \left(\frac{\breve{k}_s + \breve{k}_f}{2 \, \breve{k}_f} \right)}{1 - \phi + 2 \, \phi \left(\frac{\breve{k}_s}{\breve{k}_s - \breve{k}_f} \right) \ln \left(\frac{\breve{k}_s + \breve{k}_f}{2 \, \breve{k}_f} \right)} \right) N'(0) \end{array} \right\} \tag{18}$$

2.2. Mathematical Analysis

Consideration of SWCNTs-H_2O and MWCNTs-H_2O is a tedious, highly nonlinear, and coupled system of ODEs. In such situations, the analytical solutions are not reliable or do not even exist. Therefore, numerical techniques are better to tackle the model. Thus, the coupling of RK and shooting techniques ([14,15,30]) is adopted to capture the behavior of nanofluids flow regimes for multiple physical quantities. In ordered to initiate the algorithm, the following transformations are required depending upon the order of the self-similar momentum and energy equations described in Equations (12) and (13) along with boundary domains embedded in Equations (14) and (15). These transformations reduced the model into first order initial value problem which is then solved:

$$\breve{h}_1 = L, \breve{h}_2 = L', \breve{h}_3 = L'', \breve{h}_4 = L''' \; \breve{h}_5 = N, \breve{h}_6 = N', \tag{19}$$

From Equation (19),

$$\breve{h}_1' = L', \breve{h}_2' = L'', \breve{h}_3' = L''', \breve{h}_4' = L'''' \; \breve{h}_5' = N', \breve{h}_6' = N'', \tag{20}$$

From Equations (19) and (20), we obtained;

$$\breve{h}_1' = \breve{h}_2, \breve{h}_2' = \breve{h}_3, \breve{h}_3' = \breve{h}_4, \breve{h}_4' = L'''' \; \breve{h}_5' = \breve{h}_6, \breve{h}_6' = N'', \tag{21}$$

In Equation (21), L'''' and N'' are obtained by rearranging Equations (12) and (13) as below;

$$\begin{array}{l} L'''' = - \left(\frac{2}{K + \eta} \, L''' + (K + \eta)^{-3} L' + \dfrac{(1 - \phi) + \frac{\phi \breve{\rho}_{cnt}}{\breve{\rho}_f}}{(1 - \phi)^{-2.5}} \left\{ K(K + \eta)^{-1} (LL''' - L'L'') \right. \right. \\[3mm] \left. \left. + K(K + \eta)^{-2} \left(LL'' - L'^2 \right) - K(K + \eta)^3 LL' - \beta^* (K + \eta)^{-1} \left(L' + \frac{\eta}{2} L'' \right) - \frac{\beta^*}{2} (3L'' + \eta L''') \right\} \right), \end{array} \tag{22}$$

$$N'' \left(\frac{1 - \frac{\breve{k}_f}{\breve{k}_s} \frac{L}{R} \, \phi^{0.2} + \left(1 - \frac{\breve{k}_f}{\breve{k}_s}\right)\phi \frac{L}{R} \, \phi^{0.2} + 2 \, \phi \frac{\breve{k}_s}{\breve{k}_s - \breve{k}_f} \ln\left(\frac{\breve{k}_s + \breve{k}_f}{2 \, \breve{k}_f}\right)}{1 - \phi + 2 \, \phi\left(\frac{\breve{k}_s}{\breve{k}_s - \breve{k}_f}\right)\ln\left(\frac{\breve{k}_s + \breve{k}_f}{2 \, \breve{k}_f}\right)} \right)$$

$$= - \left(\left(\frac{\dfrac{1 - \frac{\breve{k}_f}{\breve{k}_s} \frac{L}{R} \, \phi^{0.2} + \left(1 - \frac{\breve{k}_f}{\breve{k}_s}\right)\phi \frac{L}{R} \, \phi^{0.2} + 2 \, \phi \frac{\breve{k}_s}{\breve{k}_s - \breve{k}_f} \ln\left(\frac{\breve{k}_s + \breve{k}_f}{2 \, \breve{k}_f}\right)}{1 - \phi + 2 \, \phi\left(\frac{\breve{k}_s}{\breve{k}_s - \breve{k}_f}\right)\ln\left(\frac{\breve{k}_s + \breve{k}_f}{2 \, \breve{k}_f}\right)} N'}{(K + \eta)} \right) + \right.$$

$$\left. \left\{ (1 - \phi) + \frac{\phi\left(\overline{\rho \breve{C}_p}\right)_{cnt}}{\left(\overline{\rho \breve{C}_p}\right)_f} \right\} \Pr\left(0.5 N' \beta^* + K(K + \eta)^{-1} L N' \right) \right). \tag{23}$$

Or,

$$N'' = \frac{\left(\dfrac{-\dfrac{\dfrac{1 - \frac{\breve{k}_f}{\breve{k}_s} \frac{L}{R} \, \phi^{0.2} + \left(1 - \frac{\breve{k}_f}{\breve{k}_s}\right)\phi \frac{L}{R} \, \phi^{0.2} + 2 \, \phi \frac{\breve{k}_s}{\breve{k}_s - \breve{k}_f} \ln\left(\frac{\breve{k}_s + \breve{k}_f}{2 \, \breve{k}_f}\right)}{1 - \phi + 2 \, \phi\left(\frac{\breve{k}_s}{\breve{k}_s - \breve{k}_f}\right)\ln\left(\frac{\breve{k}_s + \breve{k}_f}{2 \, \breve{k}_f}\right)} N'}{(K + \eta)} + \left\{(1 - \phi) + \frac{\phi\left(\overline{\rho \breve{C}_p}\right)_{cnt}}{\left(\overline{\rho \breve{C}_p}\right)_f}\right\} \Pr\left(0.5 N' \beta^* + K(K+\eta)^{-1} L N'\right)} \right)}{\left(\dfrac{1 - \frac{\breve{k}_f}{\breve{k}_s} \frac{L}{R} \, \phi^{0.2} + \left(1 - \frac{\breve{k}_f}{\breve{k}_s}\right)\phi \frac{L}{R} \, \phi^{0.2} + 2 \, \phi \frac{\breve{k}_s}{\breve{k}_s - \breve{k}_f} \ln\left(\frac{\breve{k}_s + \breve{k}_f}{2 \, \breve{k}_f}\right)}{1 - \phi + 2 \, \phi\left(\frac{\breve{k}_s}{\breve{k}_s - \breve{k}_f}\right)\ln\left(\frac{\breve{k}_s + \breve{k}_f}{2 \, \breve{k}_f}\right)} \right)} \tag{24}$$

Now, the resultant initial value problem is attained by including the values from Equations (19) and (21) in Equations (22) and (24). Then, this was solved successfully by means of Mathematica software 10.0.

3. Physical Interpretation of the Results

3.1. The Velocity Distribution

This section describes the results for velocity, temperature, shear stresses, and local heat transfer rate by altering the parameters concealed in the velocity and energy equation. How the volume fraction affects the thermal and physical characteristics of the host fluid and carbon nanotubes is also explored. Furthermore, the impacts of the length and radius of the carbon nanotubes are investigated for the enhancement of thermal conductivity.

The behavior of velocity against suction S > 0 and stretching and shrinking of the surface ($\lambda > 0$ and $\lambda < 0$) are captured in Figure 2. It is perceived that the nanofluid velocity declines for a larger stretching parameter. Physically, larger stretching surface parameters produce more free space and the nanofluid particles are scattered at the surface therefore the velocity $L'(\eta)$ drops. The decreasing behavior of MWCNTs-H_2O is quite abrupt in comparison with SWCNTs-H_2O. The reason behind these trends in the velocity are their densities. The nanofluid velocity asymptotically vanishes apart from the surface. On the other side, the velocity $L'(\eta)$ enhances when the surface shrinks. Physically, when the surface shrinks then the curvature decreases and, consequently, the velocity increases. This behavior of the velocity $L'(\eta)$ is shown in Figure 2a.

The influences of surface curvature on the nanofluid velocity are captured in Figure 2b. It is perceived that the nanofluid velocity $L'(\eta)$ enhances for more stretching and larger curvature of the surface. Physically, the fluid particles adjacent to the surface drag when the surface stretches, therefore the velocity of the nanofluid increases. For smaller curvature, slow increment in the velocity behavior is captured. The velocity of SWCNTs-H_2O and MWCNTs-H_2O nanofluids asymptotically vanishes beyond $\eta \geq 4.0$.
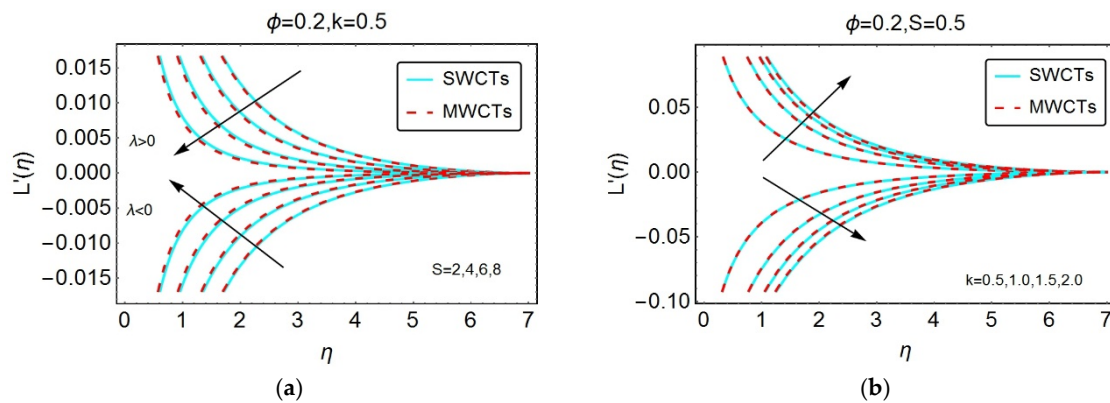
Figure 2. The velocity behavior $L\prime(\eta)$ for (**a**) suction and (**b**) curvature parameters.

The velocity of SWCNTs-H_2O and MWCNTs-H_2O against λ_1 for stretching and shrinking is painted in Figure 3. The reversal behavior of the velocity is examined for higher values of λ_1. Further, it is noted that the nanofluid flows slowly for stretching while abrupt increasing trends are seen for the shrinking case. Asymptotic behavior of the velocity $L'(\eta)$ is detected beyond $\eta \geq 5.0$ for both SWCNTs-H_2O and MWCNTs-H_2O nanofluids.
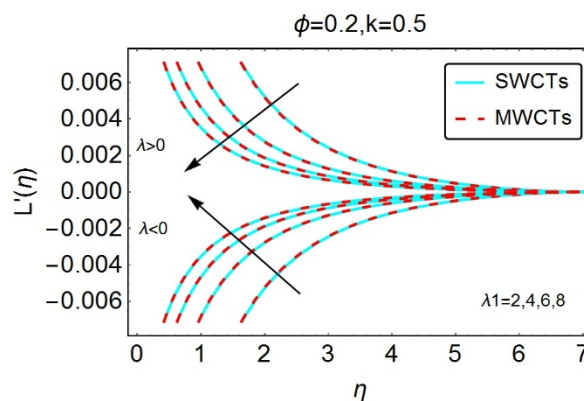
Figure 3. The velocity behavior $L\prime(\eta)$ for velocity parameter λ_1.

3.2. Streamlines and Thermophysical Characteristics

The influence of parameters concealed in the streamlines pattern and the effective thermal conductivity for CNTs, effective density, and heat capacitance are incorporated in this subsection. The parameter $\alpha > 0$ highlights the accelerated flow and decelerated flow corresponds to negative α.

Figure 4 portrays the flow pattern for accelerated and decelerated cases by keeping the surface curvature k = 4. In Figure 4a, the streamlines pattern is parabola opening downward over a curved surface. The flow is accelerated due to positive α. The streamlines expand at the free surface. It is investigated that there is no intersection of the streamlines which elaborates the phenomena of laminar flow. Figure 4b describes the flow pattern for the decelerated case. In the decelerated situation, the streamlines stretch towards a curved surface. The streamlines in the vicinity of the surface are exactly a parabolic shaped and far from the surface these become steeper. The streamlines behavior for larger surface curvature is depicted in Figure 5 for both accelerated and decelerated situations. The surface has the property of stretching which increases the surface curvature. Due to large curvature, the nanofluids flow over the surface along large curve which shrinks the streamlines pattern. An almost similar flow pattern is investigated for k = 8 in comparison with k = 4 for the decelerated case.

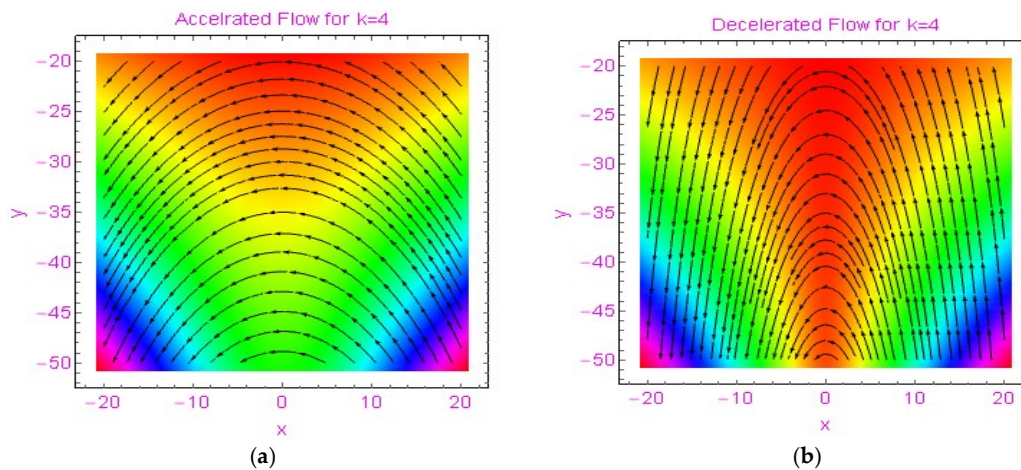**Figure 4.** Streamlines behavior for (**a**) accelerated, (**b**) decelerated flow situations when k-4.
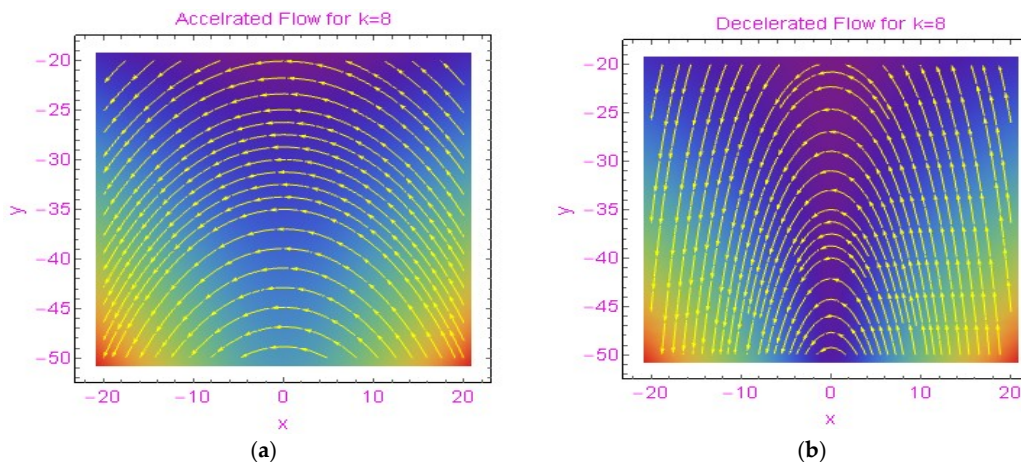

Figure 5. Streamlines behavior for (**a**) accelerated and (**b**) decelerated flow situations when k = 8.

Figure 6 elucidates the impact of suction of nanofluid for accelerated and decelerated flow situations. Under the accelerated condition, the parabolic streamlines shrink towards x = 0. The nanofluid layers slide over one another rapidly. On the other side, for a decelerating nanofluid, the layers stretch rapidly in the locality of x = 0. Figure 7 elucidates the flow pattern for injecting nanofluids. By injecting the nanofluids, the streamlines open about x = 0. The streamlines stretch for the decelerated case quite rapidly in comparison with the accelerated case.
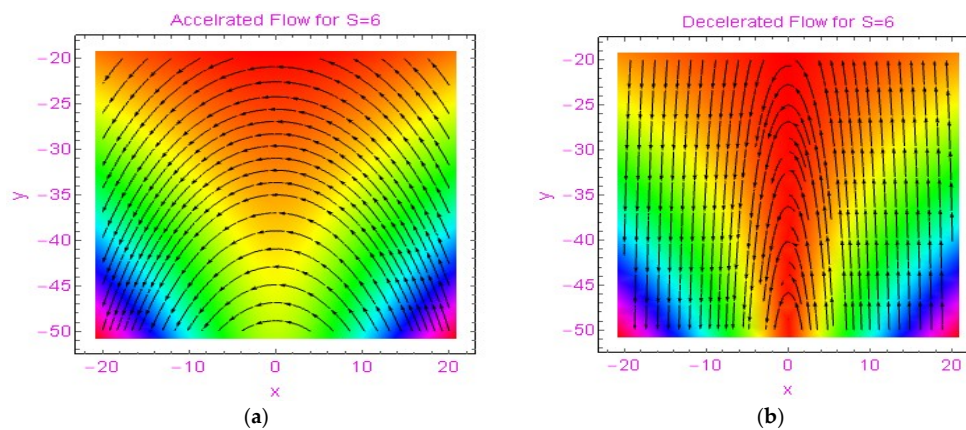

Figure 6. Streamlines behavior for (**a**) accelerated and (**b**) decelerated flow situations when S = 6.

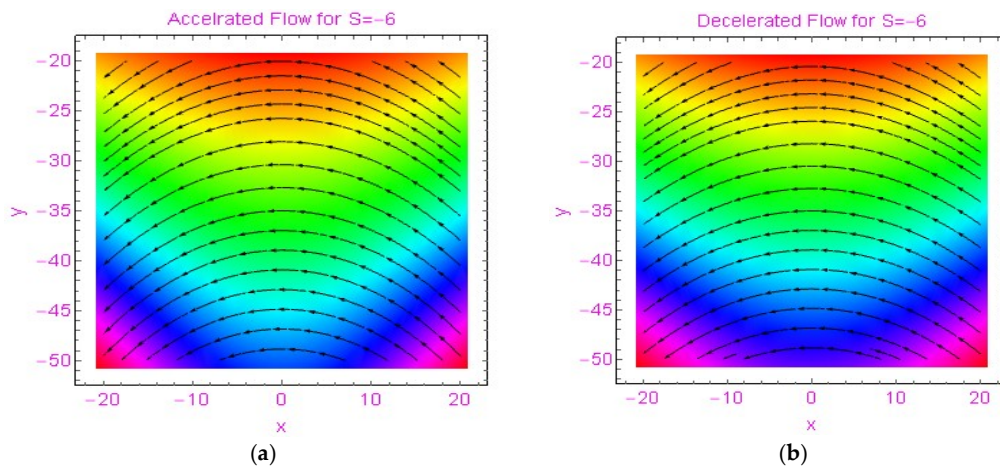(a)   (b)

Figure 7. Streamlines behavior for (**a**) accelerated and (**b**) decelerated flow situations when S = −6.

The impacts of length, radius, and volume fraction of CNTs on thermal conductivity of SWCNTs and MWCNTs are shown in Figure 8. High volume fraction of CNTs increases thermal conductivity of SWCNTs and MWCNTs. It is investigated that thermal conductivity for MWCNTs arises very rapidly in comparison with SWCNTs. The volume fraction φ is in direct proportion to thermal conductivity of CNTs. Like volume fraction, the length of the carbon nanotubes also favors the thermal conductivity for both types of carbon nanotubes. Less thermal conductivity is observed for a smaller length of carbon nanotubes. The radius of carbon nanotubes opposes the thermal conductivity. The carbon nanotubes having a larger diameter opposes the thermal conductivity. However, thermal conductivity of the carbon nanotubes can be enhanced for smaller diameters.
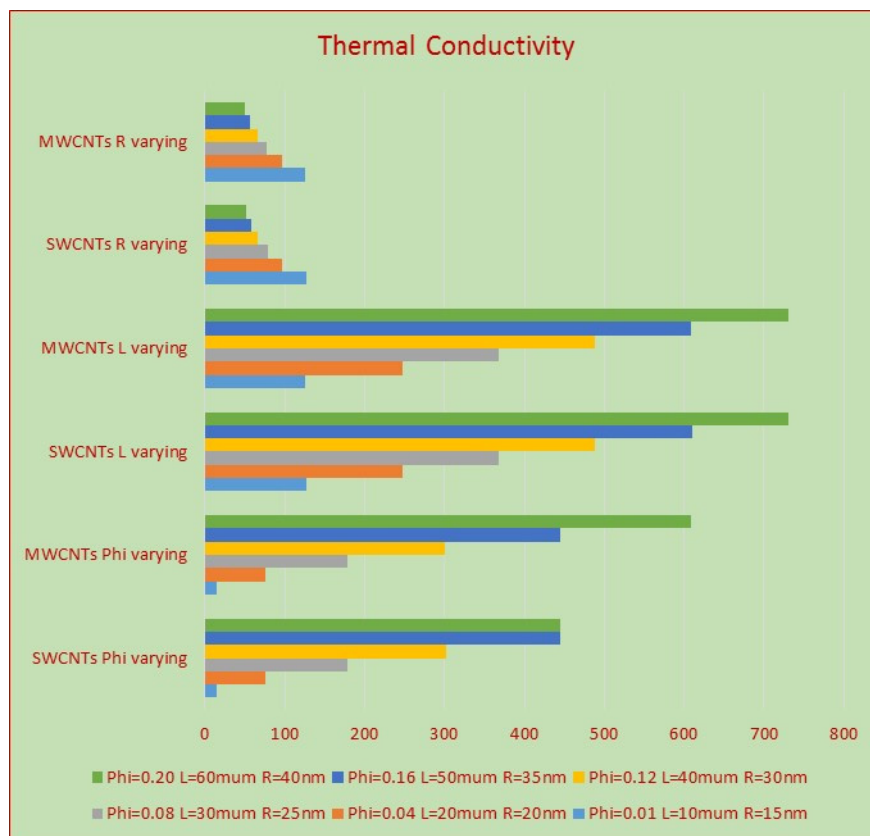

Figure 8. The behavior of thermal conductivity of SWCNTs and MWCNTs for multiple volume fraction factor φ.

The volume fraction which has a central role in the study of nanofluids is very significant for heat capacity of the nanofluids. These influences are shown in Figure 9. For smaller values of φ, heat capacity rises very rapidly. The high-volume fraction opposes the effective heat capacity of the carbon nanotubes. The relation of φ and effective density of the carbon nanotubes is in direct proportion. The density of the carbon nanotubes increases for high volume fraction. These effects are elucidated in Figure 10.
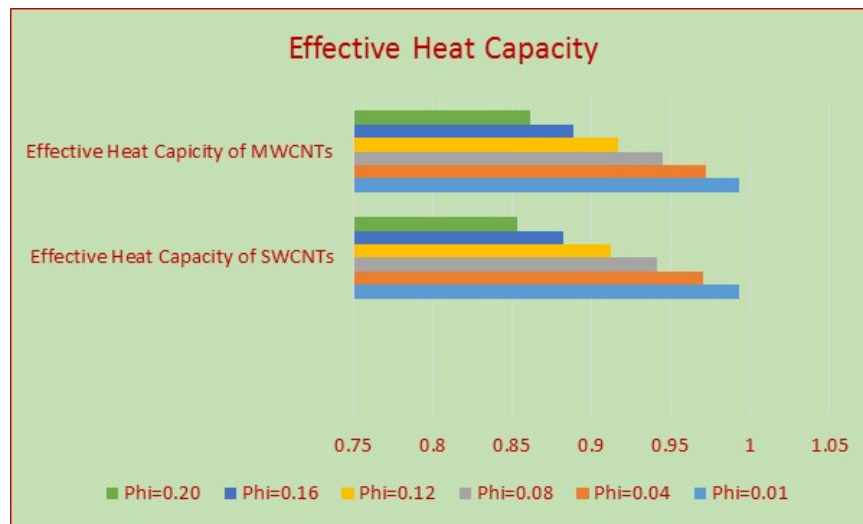

Figure 9. The behavior of heat capacity of SWCNTs and MWCNTs for multiple volume fraction factor φ.
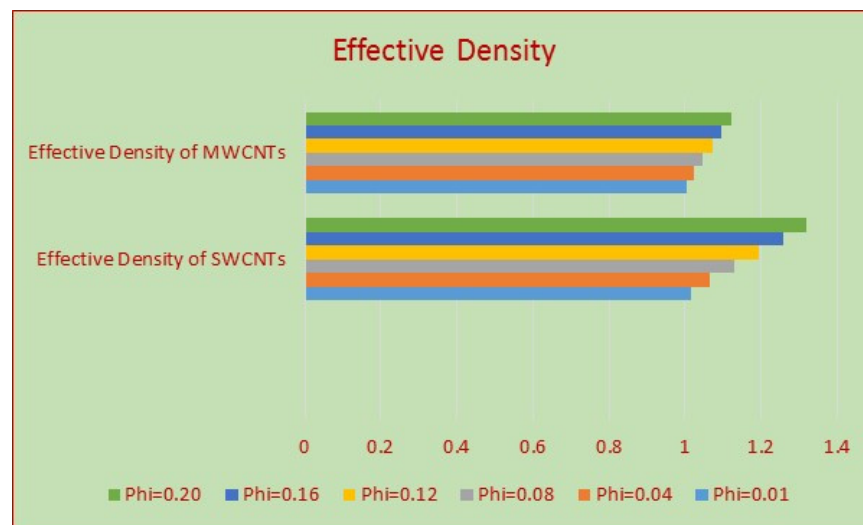

Figure 10. The behavior of density of SWCNTs and MWCNTs for multiple volume fraction factor φ.

3.3. Local Heat Transfer Rate and Skin Friction

Local Nusselt number or simply local heat transfer rate and skin friction are important quantities from an industrial point of view. The significance of these quantities cannot be denied due to industrial usage.

Figure 11 depicts the heat transfer rate versus curvature, suction of the nanofluid, and stretching of the surface. The heat transfers at the surface drops for larger curvature and enhances for smaller curvature. For SWCNTs-H_2O, nanofluid is better for more heat transfer. The larger impacts were inspected for suction of the nanofluid. For higher suction of the nanofluids, more fluid particles transfer at the surface which intensify the heat at the surface. The intensifications in the heat transfer

are almost alike. The heat transfer and stretching ($\lambda > 0$) of the surface are in assisting condition. For a more stretched surface, there is a larger amount of the heat flow at the surface. The more escalations in the heat transfer were observed for the SWCNTs-H_2O nanofluid.
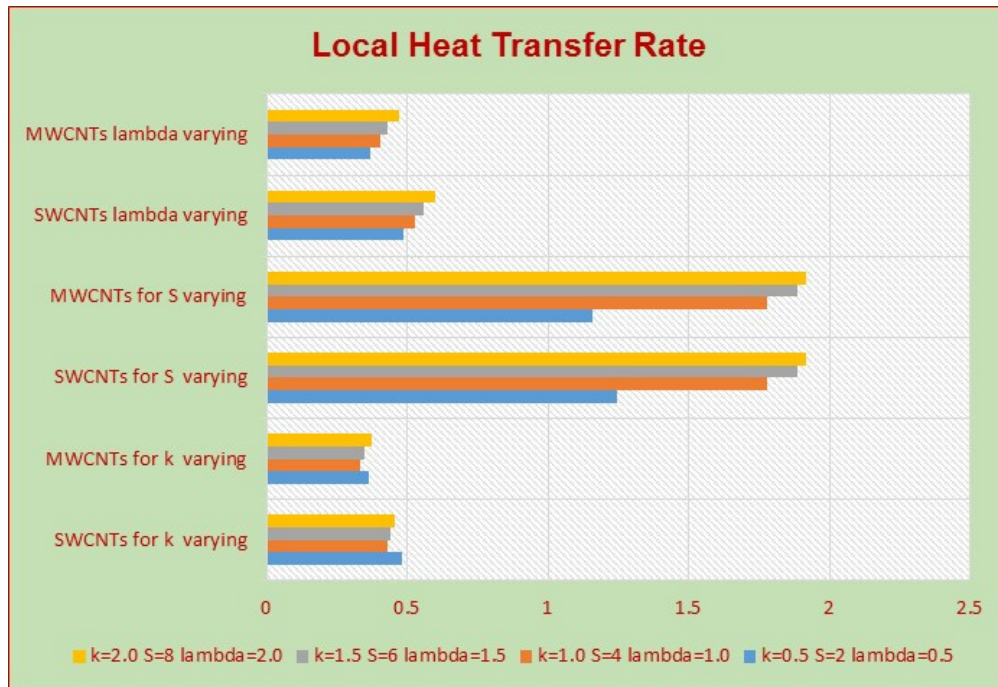

Figure 11. The behavior local Nusselt number for multiple values of k, S, and λ.

The fluctuations in the shear stresses by altering curvature, suction of the nanofluids, and stretching parameters are elucidated in Figure 12. The shear stresses escalate for the less stretched surface. Higher stretching surfaces lead to drops in the shear stresses. Similarly, the skin friction drops for more suction. The variations in the skin friction for SWCNTs-H_2O are rapid in comparison with the MWCNTs-H_2O nanofluid. The curvature parameters and the friction are inversely proportional to each other. By decreasing the curvature of the surface, the skin friction escalated, and dominant behavior is observed for the SWCNTs-H_2O nanofluid.
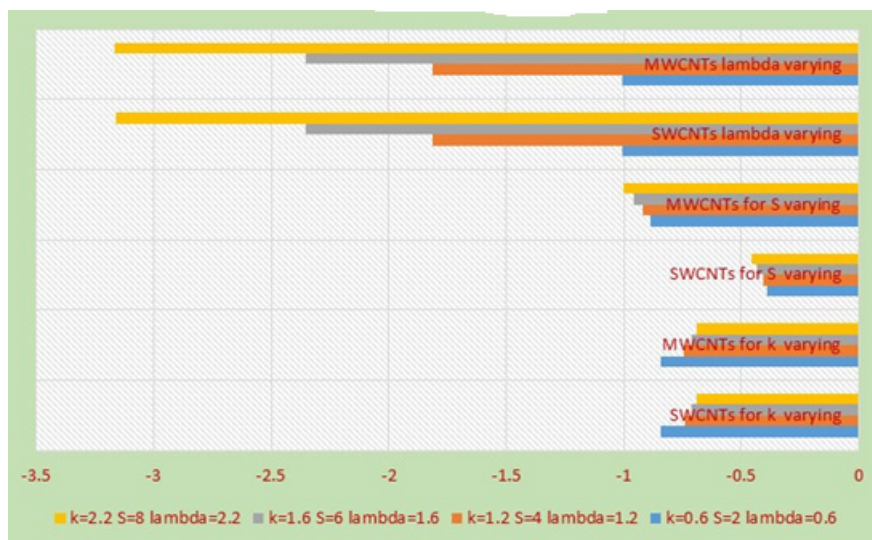

Figure 12. The behavior of shear stresses for multiple values of k, S, and λ.

4. Conclusions

Thermal transport investigation in colloidal suspension of water suspended by carbon nanomaterials was examined over curved geometry. To improve the thermal transportation in the nanofluid, a thermal conductivity correlation comprising the effects of length and radius of carbon nanomaterials was plugged into the energy equation. Then, the colloidal model was treated numerically and captured the results for the velocity, local thermal transport, and shear stresses against multiple physical parameters. It was found that:

- The stretching of the surface provides more flowing area, due to which the nanofluid particles scattered at the surface and, consequently, the velocity of the nanofluids declines over the surface.
- The nanofluids flow abruptly over a shrinking surface and asymptotically vanish apart from the surface.
- The greater heat transfer rate at the surface is perceived for the suction and stretching/shrinking parameters.
- The decreasing trends in the shear stresses over the curved surface are examined for larger curvature, whereas they increase for the stretching/shrinking and suction parameters.

Author Contributions: U.K. and A. formulated the model, N.A. and T.A. tackled the model numerically, acquired funding, and revised the manuscript, and S.T.M.-D. and I.K. wrote the results and discussion. All authors have read and agreed to the published version of the manuscript.

Conflicts of Interest: There is no conflict of interest regarding this publication.

Abbreviations

L	length of carbon nanotubes
d	diameter of carbon nanotubes
CNT	carbon nanotubes
CuO	copper oxide
SWCNTs	single walled carbon nanotubes
MWCNTs	multi walls carbon nanotubes
ODEs	ordinary differential equations
RK	Runge–Kutta scheme

References

1. Maxwell, J.C.A. *Treatise on Electricity and Magnetism*; Clarendon Press: Oxford, UK, 1881.
2. Choi, S. Enhancing Thermal Conductivity of Fluids with Nanoparticles in Developments and Applications of Non-Newtonians Flows. *ASME* **1995**, *66*, 99–105.
3. Hamilton, H.L.; Crosser, O.K. Thermal Conductivity of Heterogeneous Two-Component Systems. *Ind. Eng. Chem. Fundam.* **1962**, *1*, 187–191. [CrossRef]
4. Bruggeman, D.A.G. Berechnung verschiedener physikalischer konstanten von heterogenen substanzen, I—Dielektrizitatskonstanten und leitfahigkeiten der mischkorper aus isotropen substanzen. *Ann. Phys. Leipz.* **1935**, *24*, 636–679. [CrossRef]
5. Wasp, E.J.; Kenny, J.P.; Gandhi, R.L. Solid–liquid flow slurry pipeline transportation. *Trans Tech. Publ.* 1977, 4. Available online: https://books.google.com.pk/books/about/Solid_liquid_flow_slurry_pipeline_transp.html?id=zO1SAAAAMAAJ&redir_esc=y. (accessed on 10 May 2020).
6. Koo, J.; Kleinstreuer, C. A new thermal conductivity model for nanofluids. *J. Nanopart. Res.* **2004**, *6*, 577–588. [CrossRef]
7. Koo, J.; Kleinstreuer, C. Laminar nanofluid flow in micro-heat sinks. *Int. J. Heat Mass Transf.* **2005**, *48*, 2652–2661. [CrossRef]
8. Li, C.H.; Peterson, G.P. Experimental investigation of temperature and volume fraction variations on the effective thermal conductivity of nanoparticle suspensions (nanofluids). *J. Appl. Phys.* **2006**, *99*, 084314. [CrossRef]

9. Patel, H.E.; Sundararajan, T.; Das, S.K. An experimental investigation into the thermal conductivity enhancement in oxide and metallic nanofluids. *J. Nanopart. Res.* **2010**, *12*, 1015–1031. [CrossRef]

10. Godson, R.L.; Mohan, L.B.; Wongwises, D.S. Experimental investigation on the thermal conductivity and viscosity of silver—Deionized water nanofluid. *Exp. Heat Transf.* **2010**, *23*, 317–332. [CrossRef]

11. Corcione, M. Rayleigh–Bénard convection heat transfer in nanoparticle suspensions. *Int. J. Heat Fluid Flow* **2011**, *32*, 65–77. [CrossRef]

12. Sheikholeslami, M.; Li, Z.; Shamlooei, M. Nanofluid MHD natural convection through a porous complex shaped cavity considering thermal radiation. *Phys. Lett. A* **2018**, *382*, 1615–1632. [CrossRef]

13. Sheikholeslami, M.; Zia, Q.M.Z.; Ellahi, R. Influence of Induced Magnetic Field on Free Convection of Nanofluid Considering Koo-Kleinstreuer-Li (KKL) Correlation. *Appl. Sci.* **2016**, *6*, 324. [CrossRef]

14. Khan, U.; Adnan, A.N.; Mohyud-Din, S.T. 3D Squeezed Flow of γAl_2O_3-H_2O and γAl_2O_3-$C_2H_6O_2$ Nanofluids: A Numerical Study. *Int. J. Hydrogen Energy* **2017**, *42*, 24620–24633. [CrossRef]

15. Ahmed, N.; Adnan, K.U.; Mohyud-Din, S.T. Influence of an Effective Prandtl number Model on Squeezed Flow of $\gamma Al2O3$-H2O and γAl_2O_3-$C_2H_6O_2$ Nanofluids. *J. Mol. Liq.* **2017**, *238*, 447–454. [CrossRef]

16. Adnan, A.M.; Khan, U.; Ahmed, N.; Mohyud-Din, S.T. Analytical and Numerical Investigation of Thermal Radiation effects on Flow of viscous Incompressible fluid with Stretchable Convergent/divergent Channels. *J. Mol. Liq.* **2016**, *224*, 768–775. [CrossRef]

17. Iijima, S. Helical microtubules of graphitic carbon. *Nature* **1991**, *354*, 56–58. [CrossRef]

18. Yamada, E.; Ota, T. Effective Thermal conductivity of dispersed materials. *Heat Mass Transf.* **1980**, *13*, 27–37. [CrossRef]

19. Xue, Q.Z. Model for Thermal conductivity of carbon nanotubes-based composites. *Phys. Condens. Matter* **2005**, *17*, 1655–1660. [CrossRef]

20. Nadeem, S.; Khan, A.U.; Hussain, S.T. Model based study of SWCNT and MWCNT thermal conductivities effect on the heat transfer due to the oscillating wall conditions. *Int. J. Hydrogen Energy* **2017**, *42*, 28945–28957. [CrossRef]

21. Ahmed, N.; Adnan, K.U.; Mohyud-Din, S.T. Influence of Thermal Radiation and viscous dissipation on squeezed flow of water between two Riga plates saturated with carbon nanotubes. *Colloids Surf. A* **2017**, *522*, 389–398. [CrossRef]

22. Khan, U.; Ahmed, N.; Mohyud-Din, S.T. Heat transfer effects on carbon nanotubes suspended nanofluid flow in a channel with non-parallel walls under the effect of velocity slip boundary condition: A numerical study. *Neural Comput. Appl.* **2017**, *28*, 37–46. [CrossRef]

23. Saba, F.; Ahmed, N.; Hussain, S.; Khan, U.; Mohyud-Din, S.T.; Darus, M. Thermal Analysis of Nanofluid Flow over a Curved Stretching Surface Suspended by Carbon Nanotubes with Internal Heat Generation. *Appl. Sci.* **2018**, *8*, 395. [CrossRef]

24. Reddy, J.V.R.; Sugunamma, V.; Sandeep, N. Dual solutions for nanofluid flow past a curved surface with nonlinear radiation, Soret and Dufour effects. *J. Phys.* **2018**, *1000*, 012152. [CrossRef]

25. Saleh, S.H.M.; Arifin, N.M.; Nazar, R.; Pop, I. Unsteady Micropolar Fluid over a Permeable Curved Stretching Shrinking Surface. *Math. Probl. Eng.* **2017**, *2017*, 1–13. [CrossRef]

26. Wang, C.Y. The three-dimensional flow due to a stretching flat surface. *Phys. Fluids* **1984**, *27*, 1915–1917. [CrossRef]

27. Wang, C.Y. Fluid flow due to a stretching cylinder. *Phys. Fluids* **1988**, *31*, 466–468. [CrossRef]

28. Sakiadis, B.C. Boundary-layer behavior on continuous solid surfaces: I. Boundary-layer equations for two-dimensional and axisymmetric flow. *AIChE J.* **1961**, *7*, 26–28. [CrossRef]

29. Nadeem, U.S.; Adnan, K.U. Stability analysis of Cu-H_2O nanofluid over a curved stretching/shrinking sheet: Existence of dual solutions. *Can. J. Phys.* **2018**, *97*, 911–922. [CrossRef]

30. Ahmed, N.; Khan, A.U.; Mohyud-Din, S.T. Unsteady Radiative Flow of Chemically reacting Fluid over a Convectively Heated Stretchable Surface with Cross-Diffusion Gradients. *Int. J. Therm. Sci.* **2017**, *121*, 182–191. [CrossRef]